Frequency calibration in the ArF excimer laser-tuning range using laser-induced fluorescence of NO

Michel Versluis, Maarten Ebben, Marcel Drabbels, and J. J. ter Meulen

A frequency calibration in the tuning range of the ArF excimer laser near 193 nm was performed. Different electronic spectra of NO were measured by laser-induced fluorescence in a cell and in an oxyacetylene flame. Spectra were measured with a frequency-doubled and Raman-shifted dye laser system and with a tunable ArF excimer laser with a modified configuration. A list of absolute frequencies of the $B\,^2\Pi(v' = 7) \leftarrow X\,^2\Pi(v'' = 0)$ and $D\,^2\Sigma^+(v' = 0) \leftarrow X\,^2\Pi(v'' = 1)$ transitions in this spectral region is given, including a more comprehensive assignment of the latter excitation spectrum.

Key words: Frequency calibration, tunable excimer laser, nitric oxide.

Introduction

In the past few years there has been a growing interest in the application of tunable excimer lasers in combustion[1–3] and flow diagnostics.[4] Because of its high power, high repetition rate, and high spectral brightness, the laser allows for density and temperature field measurements at atmospheric, or even higher, pressures.[5,6] In addition, new spectroscopic information on diatomic molecules[2,7] is gathered in the tuning range of the ArF excimer laser, a frequency region that is accessible to conventional dye lasers only with a great effort. For spectroscopic reasons the need for a frequency calibration is evident. This can be achieved by absorption, fluorescence, or ionization in a gas sample contained in a calibration cell. Several stable molecules, such as O_2, H_2, CO, and NO, have electronic one- or two-photon transitions in this frequency region. Both resonance-enhanced multiphoton ionization[8] and laser-induced fluorescence[9] (LIF) can be applied as detection techniques for H_2. Four rotational lines of the $E, F \leftarrow X$ transition lie within the gain profile of the ArF excimer laser. The $B\,^3\Sigma_u^-(v' = 4)$ state of O_2, reached by excitation in the Schumann–Runge band, is a predissociating state. Consequently, the lines are broadened to several wave numbers, making them less suitable for calibration. CO, as Meijer *et al.*[7] pointed out, is well suited for frequency calibration because the transitions of this molecule are accurately measured and well tabulated. Typically, 30 mJ of laser output, however, is required for measurement of LIF of the forbidden $a\,^3\Pi(v' = 2) \leftarrow X\,^1\Sigma^+(v'' = 0)$ transition.

NO has three different electronic transitions [$A\,^2\Sigma^+(v' = 3) \leftarrow X\,^2\Pi(v'' = 0)$, $D\,^2\Sigma^+(v' = 0) \leftarrow X\,^2\Pi(v'' = 1)$, $B\,^2\Pi(v' = 7) \leftarrow X\,^2\Pi(v'' = 0)$] lying within the wavelength region near 193 nm. Both LIF[10] and resonant two-photon ionization[11] can be applied in a cell experiment. Recently Robie *et al.*[11] measured the resonant two-photon ionization spectrum of NO for frequency calibration and determination of the bandwidth of the laser. The accuracy of the line positions is, however, limited to ± 0.5 cm^{-1} because of the alinearity of their frequency scales. The assignment is confusing because of the high density of lines in the spectrum. The ionization from the A and D states is efficient, but the ground-state levels are not well populated at room temperature. The transitions that can be excited by the ArF laser start from $J = 30.5$ for the $A \leftarrow X$ band and from a vibrationally excited level for the $D \leftarrow X$ transition. Consequently the overall ion yield is low in both cases. LIF spectroscopy of these states is difficult for the same reason. The ionization cross section from the B state is rather small,[12] making LIF from this state most preferable in a cell experiment. The $D \leftarrow X$ transition can also be used for calibration if the NO molecules are measured in a flame. The $B \leftarrow X$ and $A \leftarrow X$ transitions are not observed in the flame experiment because of quench-

The authors are with the Department of Molecular and Laser Physics, University of Nijmegen, Toernooiveld, NL-6525 ED Nijmegen, The Netherlands.

Received 22 February 1991.
0003-6935/91/365229-06$05.00/0.

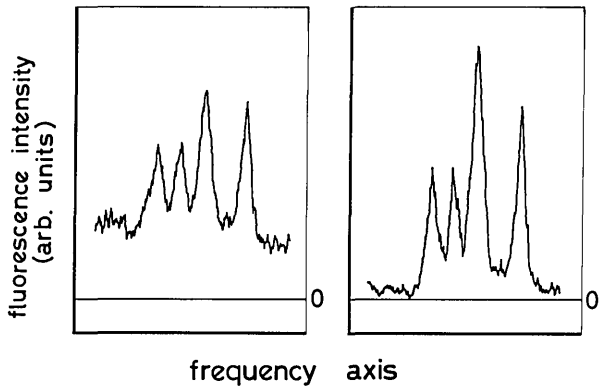

Fig. 1. Part of the NO:$D\,^2\Sigma^+ \leftarrow X\,^2\Pi$ spectrum measured with two different configurations of the excimer laser. The left-hand excitation spectrum is measured with unstable resonator (Cassegrain) optics. The right spectrum is measured without the unstable resonator optics.

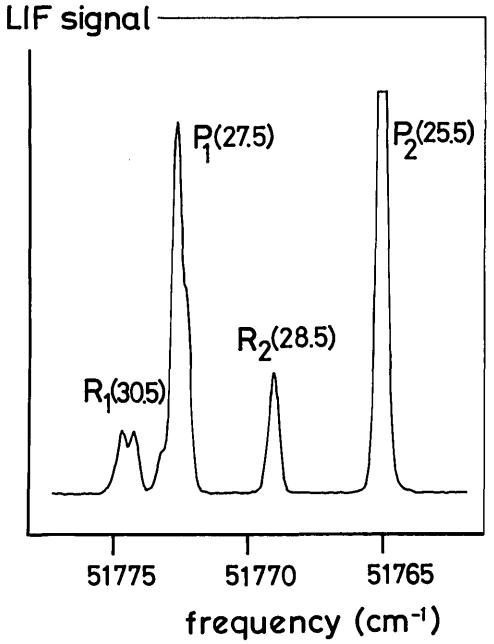

Fig. 2. Part of the NO:$B\,^2\Pi(v' = 7) \leftarrow X\,^2\Pi(v'' = 0)$ spectrum near 51 770 cm^{-1}.

ing of the fluorescence, which is due to the relatively long lifetime of the excited states, and the low abundance of NO in the flame. We chose to apply LIF in the flame experiment. For both the $B \leftarrow X$ and $D \leftarrow X$ transitions, we calibrated the line positions. A new assignment of the rotational lines belonging to the $D \leftarrow X$ transition was obtained.

Experimental Setup

The calibration cell consists of a stainless-steel vacuum chamber equipped with two Suprasil I windows (diameter 50 mm × 5 mm). A diaphragm and light baffles control the size of the laser beam and reduce stray light in the cell. NO is made to flow continuously through the cell. The flow is controlled by a needle valve. The pressure in the cell is 100 mTorr. The fluorescence is dispersed by a 0.125-m monochromator (Oriel 77250, 1200 g/mm) with a maximum resolution of 1 nm. The transmitted photons are measured with a photomultiplier (EMI 9863 B 350 ac), and the signals are time averaged with a boxcar integrator (SRS 250). Light can be detected for wavelengths above ~280 nm, so no interference of resonant laser light influences the measurements.

Flame spectra were measured in an oxyacetylene welding torch. The LIF of abundant NO is collected from a region 1–2 cm above the flame front by means of a Suprasil I lens. The fluorescence is focused onto the entrance slit of a 0.25-m-focal-length monochromator (Jobin Yvon M25, 610 g/mm, 1-nm resolution) and is detected by a photomultiplier (EMI 9635 QB). The signals are time averaged with a second boxcar integrator (SRS 250). The flame and the cell spectra are recorded simultaneously on a strip-chart recorder.

The spectra were recorded by using two laser systems. The actual calibration spectra were measured by Raman shifting a frequency-doubled tunable dye laser. The output of a Nd:YAG laser (Quantel 681-10C) was doubled to pump a dye laser (Continuum TDL 60) operating on Rhodamine 6G. The dye laser beam is frequency doubled in a KDP crystal delivering typically 30 mJ of pulse energy. This UV light is then focused with an $f = 150$ mm Suprasil I lens into a stainless-steel cell containing 15 bars of H_2, generating several Stokes and anti-Stokes beams. The fourth anti-Stokes is directed to the calibration cell by a Suprasil I prism. Less than 50 μJ of tunable 193-nm radiation is used to irradiate the gas sample contained in the calibration cell. A part of the fundamental dye-laser beam is used for I_2 absorption measurements. In this way the frequency of the vacuum-UV light could be calibrated by using I_2-frequency tables.[13] Because we want to calibrate our spectra to an accuracy of 0.1 cm^{-1}, the H_2 Raman shift has to be accurate within 0.02 cm^{-1}. The value of the Raman shift shows a pressure dependence.[14] We adopted the value of 4155.21 cm^{-1}, in agreement with the constants given in Ref. 14. Five lines of the $B \leftarrow X$ transition, three at the blue end and two at the red end of the spectrum, are measured together with the I_2 lines.

The spectra were also measured with a tunable ArF excimer laser (Lambda Physik EMG 150 MSCT). The laser consists of two discharge cavities. In the normal setup one cavity is used as an oscillator. In combination with beam-expanding prisms and a diffraction grating, a diaphragm and a circular aperture of 2-mm diameter in the resonator cavity are used for the generation of narrow-band radiation. By tilting the grating and moving its reflection along the aperture, we could tune the frequency of the oscillator within its gain profile. The other discharge cavity is used as an amplifier. The relatively small oscillator beam is expanded and amplified by means of unstable resonator (or Cassegrain) optics. Typically, 100-mJ-per-pulse tunable narrow-band radiation is achieved for ArF-optimized excimer lasers. The laser is tunable

over 200 cm^{-1} with a bandwidth of 0.4 cm^{-1}. The use of unstable resonator optics results in a beam divergence of < 0.2 mrad.

The amplification stage has some disadvantages, however, for two-dimensional fluorescence imaging and spectroscopic reasons. In the first place, the application of Cassegrain optics results in a circular (diameter 2.5 mm) intensity dip in the middle of the beam cross section. The spatially inhomogeneous distribution of pulse energy in a laser sheet, produced by cylindrical lenses, will result in misleading planar fluorescence images. Second, the amplifier discharge cavity equipped with unstable resonator optics is a lasing medium on its own, typically delivering 50 mJ of broadband energy per pulse when not injected by narrow-band oscillator radiation. If, because of decreasing oscillator power, the amplifier is not completely locked to the oscillator, the laser output will be a combination of narrow-band and broadband radiation, making spectroscopy, both LIF and resonance-enhanced multiphoton ionization, more complicated. This artifact occurs on both red and blue ends of the tuning range and every time the oscillator hits an O_2-absorption line belonging to the Schumann–Runge $B\ ^3\Sigma_u^-(v' = 4) \leftarrow X\ ^3\Sigma_g^-(v'' = 0)$ band. The spectral density of the broadband light is still 0.1 mJ/cm^{-1}, enough to induce additional (and therefore confusing) fluorescence. Removing the unstable resonator optics and guiding a wide oscillator beam in a single pass through the amplifier discharge tube would eliminate this problem.

Research by Wodtke *et al.*[2] describes insertion of rectangular apertures in the oscillator resonator of a Lambda Physik EMG 150 EST, where cylindrical

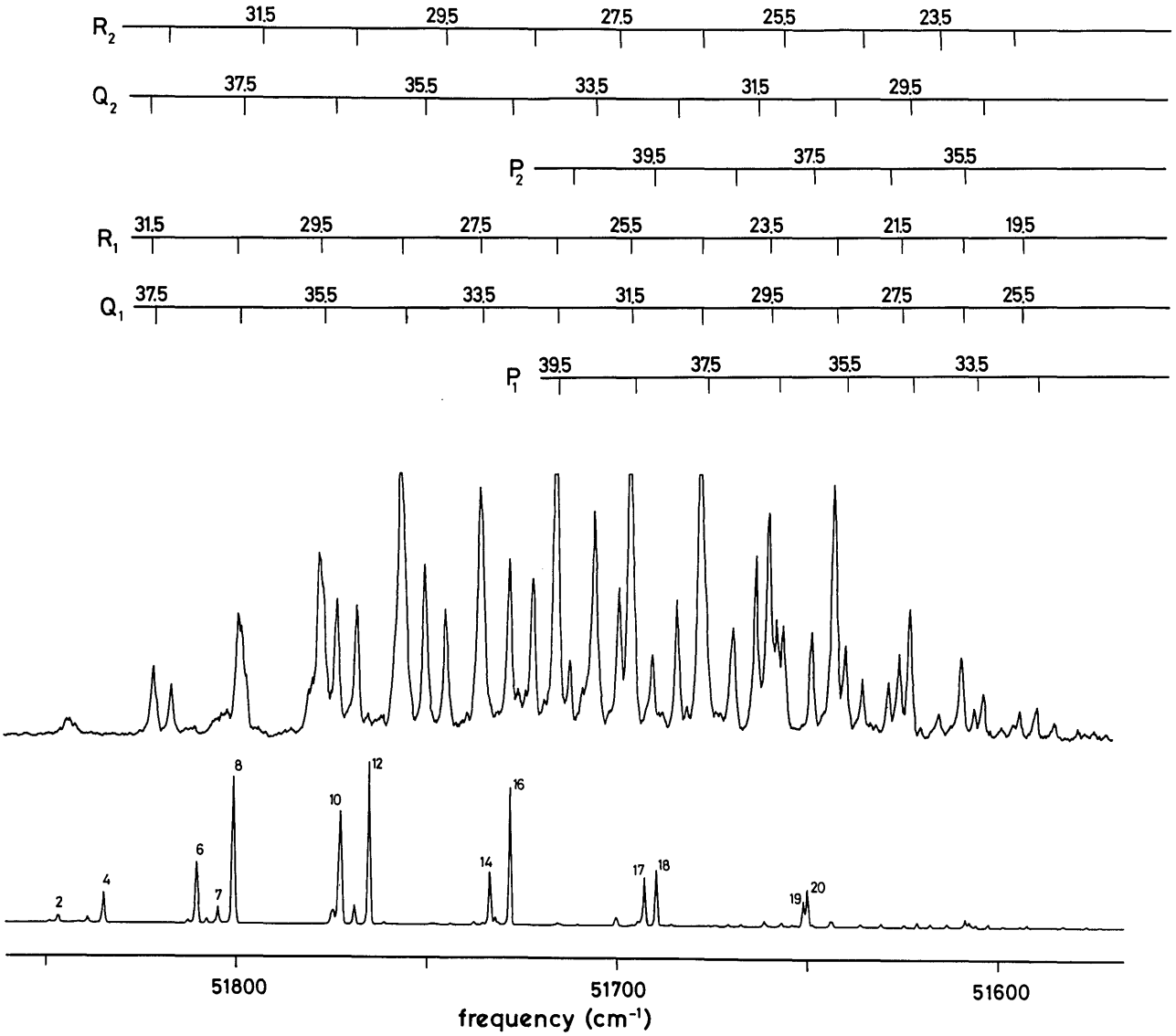

Fig. 3. Upper spectrum: The excitation spectrum of the $D\ ^2\Sigma^+(v' = 0) \leftarrow X\ ^2\Pi(v'' = 1)$ transition of natural abundant NO measured in an oxyacetylene flame. Four lines are truncated because of the limited dynamic range of the strip-chart recorder. Lower spectrum: The excitation spectrum of the $B\ ^2\Pi(v' = 7) \leftarrow X\ ^2\Pi(v'' = 0)$ transition of NO measured in a cell at a pressure of 100 mTorr. The numbers of the labeled lines in the lower spectrum correspond to the frequencies tabulated in Table I.

lenses expand the oscillator beam before injection into the amplifier. We found that removal of the diaphragm and the circular aperture did not influence the bandwidth of the oscillator. By using beam-expanding prisms of 30-mm height, one can generate an oscillator beam (dimensions, 22 mm × 4 mm) delivering 1 mJ of energy per pulse with a bandwidth of 0.4 cm^{-1}. This beam is then passed through the amplifier discharge cavity, yielding at maximum 40 mJ per pulse of tunable narrow-band radiation. The tuning range increased to 300 cm^{-1}. In combination with the absence of broadband laser emission, this modified setup is more suited for spectroscopic measurements. This is demonstrated in Fig. 1, where the same rotational lines of the NO:$D(v' = 0) \leftarrow X(v'' = 1)$ transition near 51 650 cm^{-1} are measured with the two different configurations of the ArF laser. The left-hand spectrum is measured with Cassegrain (unstable resonator) optics, whereas the right-hand one is measured without the unstable resonator optics. Notice that the offset in the left-hand spectrum is due to excitation of the NO molecules by broadband radiation, and therefore it depends on the pulse-to-pulse fluctuations of the power. Moreover, it depends

Table I. *P* and *R* lines of the $B\,^2\Pi$ ($v' = 7$) ← $X\,^2\Pi$ ($v'' = 0$) transition observed within the tuning range of the ArF laser (in cm^{-1})[a]

	Observed Frequency[b]	Transition[c]
1	51849.7	R_1 (28.5)
2	51847.8	P_1 (25.5)
3	51839.6	R_2 (26.5)
4	51835.6	P_2 (23.5)
5	51813.2	R_1 (29.5)
6	51810.9	P_1 (26.5)
7	51805.2	R_2 (27.5)
8	51801.0	P_2 (24.5)
9	51774.7	R_1 (30.5)
10	51772.7	P_1 (27.5)
11	51769.1	R_2 (28.5)
12	51765.2	P_2 (25.5)
13	51734.8	R_1 (31.5)
14	51733.0	P_1 (28.5)
15	51731.6	R_2 (29.5)
16	51727.6	P_2 (26.5)
17	51692.0	P_1 (29.5)
18	51689.2	P_2 (27.5)
19	51649.8	P_1 (30.5)
20	51648.7	P_2 (28.5)

[a]The numbers in the first column correspond to the labeled lines in the lower spectrum of Fig. 3.
[b]The observed error is 0.2 cm^{-1}.
[c]Notation: $\Delta J_{F'}(J'')$.

Table II. Absolute Frequencies of the $D^2\Sigma^+$ ($v' = 0$) ← $X^2\Pi$ ($v'' = 1$) Transition Observed in the Tuning Range of the ArF Laser (in cm^{-1})

Observed Frequency	Transition[a]	Calculated Frequency	Observed Frequency	Transition[a]	Calculated Frequency
51819.5	R_1 (31.5)	51819.7	51674.3	R_1 (24.5)	51674.4
819.5	Q_2 (38.5)	819.6	674.3	Q_1 (30.5)	674.3
819.5	Q_1 (37.5)	818.9	674.3	R_2 (26.5)	674.0
815.1	R_2 (32.5)	815.0	673.0	P_1 (37.5)	672.8
796.8	R_1 (30.5)	797.0	665.8	P_2 (38.5)	665.7
796.8	Q_1 (36.5)	796.3	659.6	Q_2 (31.5)	659.5
795.3	Q_2 (37.5)	794.9	656.2	R_1 (23.5)	656.3
Not obs.[b]	R_2 (31.5)	90.0	656.2	Q_1 (29.5)	656.2
51775.1	R_1 (29.5)	775.0	654.2	P_1 (36.5)	654.1
775.1	Q_1 (35.5)	774.4	652.6	R_2 (25.5)	652.6
771.0	Q_2 (36.5)	770.8	644.8	P_2 (37.5)	644.9
766.0	R_2 (30.5)	765.6	638.9	Q_2 (30.5)	639.0
753.5	R_1 (28.5)	753.6	638.9	R_1 (22.5)	638.7
753.5	Q_1 (34.5)	753.1	638.9	Q_1 (28.5)	638.7
747.8	Q_2 (35.5)	747.4	636.0	P_1 (35.5)	636.1
741.9	R_2 (29.5)	741.8	631.6	R_2 (24.5)	631.7
732.5	R_1 (27.5)	732.8	624.6	P_2 (36.5)	624.7
732.5	Q_1 (33.5)	732.4	621.6	Q_1 (27.5)	621.9
725.1	Q_2 (34.5)	724.5	621.6	R_1 (21.5)	621.8
718.8	R_2 (28.5)	718.6	618.9	Q_2 (29.5)	619.1
712.5	R_1 (26.5)	712.7	618.9	P_1 (34.5)	618.7
712.5	Q_1 (32.5)	712.4	611.4	R_2 (23.5)	611.5
712.5	P_1 (39.5)	712.0	605.3	Q_1 (26.5)	605.7
709.3	P_2 (40.5)	Not calc.[c]	605.3	R_1 (20.5)	605.6
702.5	Q_2 (33.5)	51702.2	605.3	P_2 (35.5)	605.1
696.2	R_1 (21.5)	696.0	601.9	P_1 (33.5)	601.9
692.8	R_2 (27.5)	693.3	599.6	Q_2 (28.5)	599.8
692.8	Q_1 (31.5)	693.0	591.7	R_2 (22.5)	591.9
692.8	P_1 (38.5)	692.1	589.5	Q_1 (25.5)	590.2
687.4	P_2 (39.5)	Not calc.[c]	589.5	R_1 (19.5)	590.0
51680.7	Q_2 (32.5)	51680.5	51585.3	P_1 (32.5)	51585.8

[a]Notation: $\Delta J_{F'}(J'')$.
[b]Not observed because of the absence of laser action resulting from intracavity absorption.
[c]Not calculated because energy levels in Ref. 17 are not calculated for such high J values.

on the fluctuating NO concentration in the flame. Because the intensity dip originating from the unstable resonator optics is no longer present, one can generate laser sheets with a homogeneous energy distribution suited for planar fluorescence imaging.

Results and Discussion

All spectra in this experiment were measured without Cassegrain optics. A part of the NO:$B\,^2\Pi(v' = 7) \leftarrow X\,^2\Pi(v'' = 0)$ spectrum, measured with the tunable excimer laser, is shown in Fig. 2. The linewidth of 0.38 cm^{-1} is determined by the bandwidth of the laser. The monochromator is set to transmit the fluorescence around 337 nm. The monochromator has a resolution of ~15 nm. The identification of the rotational lines is also indicated in Fig. 2. The splitting of the $R_1(30.5)$ line at 51775 cm^{-1} is due to the Λ-doublet splitting in the ground state. The splitting grows linearly with the quantum number J. No splitting is observed in the F_2 manifold because $^2\Pi_{3/2}$ states couple only weakly with the electronically excited Σ states.

The $B \leftarrow X$ (lower) and the $D \leftarrow X$ (upper) excitation spectra are shown in Fig. 3. These spectra were recorded simultaneously during the frequency scan. Notice the absence of the broadband wings on the extreme sides of the tuning range. Because the linearities of the grating stepper motor and the strip-chart recorder were not known, the calibration lines were fitted to a polynomial function. We found that the horizontal axis is linear with the frequency within the present accuracy. The lines of the $B \leftarrow X$ transition lying within the tuning range of the ArF laser are tabulated in Table I. The observed error of the line positions is 0.2 cm^{-1}.

For the observation of the NO:$D\,^2\Sigma^+(v' = 0) \leftarrow X\,^2\Pi(v'' = 1)$ excitation spectrum, the monochromator was set to transmit the $D(v' = 0) \rightarrow X(v'' = 3)$ fluorescence at 208 nm only. The monochromator was set to the maximum resolution (1 nm) to prevent detection of O_2 fluorescence, which is induced in the same spectral region. All lines can be assigned to P, Q, and R lines of the $D(v' = 0) \leftarrow X(v'' = 1)$ transition and are tabulated in Table II together with their assignments and calculated frequencies. It must be noted that Ref. 10 contains some misassigned lines. The calculation is performed in the following way: The energy values of the $D(v' = 0)$ state are given by the usual expression,

$$F_1(N) = T_0 + BN(N + 1) - DN^2(N + 1)^2 + \tfrac{1}{2}\gamma N, \quad (1)$$

$$F_2(N) = T_0 + BN(N + 1) - DN^2(N + 1)^2 - \tfrac{1}{2}\gamma(N + 1), \quad (2)$$

where T_0, B, and D are taken from Refs. 15 and 16. The ground-state energy values in $v'' = 1$ are taken from Ref. 17. The Λ-doublet splitting has been ignored. Frequencies are calculated by subtracting the energy values of both electronic states. The agreement between measured and calculated lines is good within the indicated error (0.2 cm^{-1}). Some lines are overlapping, which makes it difficult to determine the exact center of the line position.

Summary

We performed a frequency calibration in the tuning range of the ArF excimer laser near 193 nm. A list of absolute frequencies of the $B\,^2\Pi(v' = 7) \leftarrow X\,^2\Pi(v'' = 0)$ and the $D\,^2\Sigma^+(v' = 0) \leftarrow X\,^2\Pi(v'' = 1)$ transitions in NO is given. Both electronic transitions can be used as a calibration in this spectral region. Whether a cell or a flame experiment is used depends on the application.

We thank Maarten Boogaarts for experimental assistance. The technical assistance of Eugène van Leeuwen, Cor Sikkens, Frans van Rijn, and John Holtkamp is gratefully acknowledged. We thank Peter Andresen for many fruitful and stimulating discussions. This study has been made possible by the financial support of the Stichting voor Technische Wetenschappen and the Stichting voor Fundamenteel Onderzoek der Materie.

References

1. P. Andresen, A. Bath, W. Gröger, H. Lülf, G. Meijer, and J. J. ter Meulen, "Laser-induced fluorescence with tunable excimer lasers as a possible method for instantaneous temperature field measurements at high pressures: checks with an atmospheric flame," Appl. Opt. **27,** 365–378 (1988).
2. A. M. Wodtke, L. Hüwel, H. Schlüter, H. Voges, G. Meijer, and P. Andresen, "Predissociation of O_2 in the B state," J. Chem. Phys. **89,** 1929–1935 (1988).
3. R. Suntz, H. Becker, P. Monkhouse, and J. Wolfrum, "Two-dimensional visualization of the flame front in an internal combustion engine by laser-induced fluorescence of OH radicals," Appl. Phys. B **47,** 287–293 (1988).
4. G. Laufer and R. L. McKenzie, in presented at the Conference on Sensors and Measurements for Aeronautical Applications, 7–9 September 1988, Atlanta, Ga.
5. P. Andresen, G. Meijer, H. Schlüter, H. Voges, A. Koch, W. Hentschel, W. Oppermann, and E. Rothe, "Fluorescence imaging inside an internal combustion engine using tunable excimer lasers," Appl. Opt. **29,** 2392–2404 (1990).
6. A. Chryssostomou, H. Voges, W. Reckers, P. Andresen, P. Krogmann, K.-A. Bütefisch, and H. Wolfrum, "Two dimensional laser diagnostic experiments at the RWG wind tunnel," Rep. No. 1/340/1990 (DLR Göttingen, Laser Laboratorium Göttingen, 1990).
7. G. Meijer, A. M. Wodtke, H. Voges, H. Schlüter, and P. Andresen, J. Chem. Phys. **89,** 2588–2589 (1988).
8. E. W. Rothe, G. S. Ondrey, and P. Andresen, Opt. Commun. **58,** 113–117 (1986).
9. D. J. Kligler and C. K. Rhodes, "Observation of two-photon excitation of the H_2 E, $F\,^1\Sigma$ state," Phys. Rev. Lett. **40,** 309–313 (1978).
10. A. M. Wodtke, L. Hüwel, H. Schlüter, G. Meijer, P. Andresen, and H. Voges, "High-sensitivity detection of NO in a flame using a tunable ArF laser," Opt. Lett. **13,** 910–912 (1988).
11. D. C. Robie, J. D. Buck, and W. K. Bischel, "Bandwidth and tuning range of an ArF laser measured by 1 + 1 resonantly enhanced multiphoton ionization of NO," Appl. Opt. **29,** 3961–3965 (1990).
12. H. Rottke and H. Zacharias, "Photoionization of single rotational levels in excited $B\,^2\Pi$, $C\,^2\Pi$, and $D\,^2\Sigma^+$ states of $^{14}N^{16}O$," J. Chem. Phys. **83,** 4831–4844 (1985).

13. S. Gerstenkorn and P. Luc, *Atlas du Spectroscopie d'Absorption de la Molecule d'Iode* (Centre National de la Recherche Scientifique, Orsay, France, 1978); "Absolute iodine (I_2) standards measured by means of Fourier transform spectroscopy," Rev. Phys. Appl. **14,** 791–794 (1979).
14. J. V. Foltz, D. H. Rank, and T. A. Wiggins, "Determination of some hydrogen molecular constants," J. Mol. Spectrosc. **21,** 203–216 (1966).
15. C. Amiot and J. Verges, "Spin–rotation doubling in the NO $A\ ^2\Sigma^+$, $D^2\ \Sigma^+$, and $E^2\ \Sigma^+$ ($v = 0$) electronic states by emission Fourier transform spectroscopy," Chem. Phys. Lett. **66,** 570–573 (1979).
16. C. Amiot and J. Verges, "Fourier transform spectrometry of the $D\ ^2\Sigma^+$–$A\ ^2\Sigma^+$, $E\ ^2\Sigma^+$–$D\ ^2\Sigma^+$ and $E\ ^2\Sigma^+$–$A\ ^2\Sigma^+$ and systems of nitric oxide," Phys. Scripta **26,** 422–438 (1982).
17. A. Hinz, J. S. Wells, and A. G. Maki, "Heterodyne frequency measurements on the nitric oxide fundamental band," J. Mol. Spectrosc. **119,** 120–125 (1986).